A Fluid-Structure Interaction Finite Element Analysis of Pulsatile Blood Flow through a Compliant Stenotic Artery

by

Mark Bathe

Submitted to the Department of Mechanical Engineering in
Partial Fulfillment of the Requirements for the Degree of

Bachelor of Science

at the

Massachusetts Institute of Technology

February 1998

Signature of Author:..
Department of Mechanical Engineering
January 16, 1998

Certified by:..
Roger D. Kamm
Professor of Mechanical Engineering
Thesis Supervisor

Accepted by:...
Derek Rowell
Professor of Mechanical Engineering
Chairman, Undergraduate Thesis Committee

A Fluid-Structure Interaction Finite Element Analysis of Pulsatile Blood Flow through a Compliant Stenotic Artery

by

Mark Bathe

ABSTRACT

An axisymmetric, fully coupled, fluid-structure interaction finite element analysis of pulsatile blood flow through a compliant stenotic artery was performed, with minimum diameter reduced by either 30 or 80 percent (51 or 96 percent area reduction). Several novel modeling assumptions were incorporated into the model. Among these were an *in vivo* axial arterial stretch ratio of 1.5, constant through-thickness hoop stress at median blood pressure, and a non-linear stress-stretch curve fit to experimental data over a range of stretch spanning 1 to 1.75. While the stresses in and around the stenoses were of primary interest, the inner wall hoop strain amplitude and the development of negative post-stenotic transmural pressures were also considered.

Results show that with an 80 percent constriction peak compressive stresses reach 103 kPa in the downstream shoulder of the plaque due to the abnormal downstream contraction of the artery during times of peak blood flow. This contraction also causes the downstream inner wall arterial hoop strain amplitude to increase from 21 to 25 percent from the mild to severe constriction case. Both stenoses almost fully restrict the normal vasodilation of the artery. Despite the large maximum pressure drop (13 kPa) occurring in the 80 percent case during peak flow, no negative blood pressures developed in either model at any time, under the laminar flow assumption used in this analysis.

Thesis Supervisor: Roger D. Kamm
Title: Professor of Mechanical Engineering

Table of Contents

Table of Figures

1.0 Introduction

The role of hemodynamics in atherosclerosis is now well established. The pattern of atherosclerotic lesions bears a clear relationship to the patterns of flow and shear stress exerted by blood on the arterial lumen. In vitro studies have demonstrated that shear stress and mechanical strain can both influence the biological function, in particular the gene expression, of vascular endothelial cells, Sumpio *et al.* (1996). Fluid dynamic stress has been implicated in the rupture and progressive development of arterial stenoses and associated thrombi. For all these reasons, there has been considerable interest on the part of bioengineers and other medical researchers to better understand the nature of arterial blood flow through the use of experimental, analytical, and more recently, computational models.

Various computational approaches have been used to examine the relationship between fluid dynamic stresses and arterial disease. Focusing on the hemodynamics, studies have examined the role of flow unsteadiness and compliance, Downing and Ku (1997), Non-Newtonian properties, Tandon and Rana (1995), and turbulence, Bluestein *et al.* (1997), on the detailed flow patterns produced. Each of these studies has been limited in scope by the assumption of either a rigid vessel wall, steady flow, or one-dimensionality. Of the abovementioned studies, the only one that investigates the coupled fluid flow-structure problem is the one by Downing and Ku (1997). The main limitations to this study were that it assumed one-dimensional flow and used a highly simplified description of arterial wall mechanics. Even with these assumptions, however, this study served to illustrate the potential for strong fluid-structure coupling that might, under some circumstances, lead to collapse and possible fatigue in the region of the arterial plaque. Separate studies using a finite element analysis of hypothetical and actual stenosis geometries with separate regions of calcified plaque, lipid, and normal arterial wall by Loree *et al.* (1992) and Cheng *et al.* (1993), have shown that stresses internal to the wall associated with normal arterial pressures may be sufficient to cause the plaque cap to fracture, an event that often initiates thrombus formation contributing to further occlusion, and potentially a serious ischemic episode. This method of analysis was successful in identifying the conditions for, and sites of, wall rupture. The stress analysis in these studies, however, was two-dimensional and assumed plane strain and static conditions. No attempt was made to simulate the true fluid dynamic stresses on the arterial wall nor any of the longitudinal nor large strain effects.

The aim of this study was to combine the previously mentioned computational models into one expanded, unified model, incorporating as many physiological phenomena as possible to gain new insight into the transient stress and strain state in a stenotic artery. The model developed for this study is an axisymmetric, large strain, finite element model of a stenotic canine carotid artery, that takes into account the fully coupled fluid flow-structural interaction effects. Three pulsatile cardiac cycles are computed in which unsteady flow and transient dynamic effects are accounted for in the fluid and solid domains. An experimentally based non-linear stress-stretch material curve is used to model the arterial

5

domain. A 1.5 axial arterial stretch ratio is incorporated into the model, as well as a constant through-thickness hoop stress at median blood pressure. While the stress state in the region of the stenosis is of primary interest, inner wall hoop strain and fluid pressure distributions are also considered. The primary limitations of the study are the assumptions of laminar flow and a homogeneous, isotropic stenosis.

2.0 Governing Equations

The commercially available finite element analysis programs *ADINA* and *ADINA-F* were used in this study to solve the governing equations for solids and fluids in a fully coupled manner. The equations are presented below.

2.1 Solids

The solid model response was analyzed using the standard Lagrangian formulation. The governing field equation is:

$$^t\tau_{ij,j} = \rho\,^t\ddot{u}_i \tag{2.1}$$

where at time, *t*,

$$^t\tau_{ij} = \text{component of Cauchy stress tensor}$$
$$^t\ddot{u}_i = \text{material particle acceleration}$$

and

$$\rho = \text{constant material particle density}$$

The boundary conditions used to solve the above field equations are described in detail in *Section* 4.5.1.

Note that the strains presented in this study are Green-Lagrange strains, defined as

$$\varepsilon = (l^2 - l_0^2)/2l_0^2 \tag{2.2}$$

where for a differential fiber

$$l = \text{current fiber length}$$
$$l_0 = \text{original fiber length}$$

and as a point of reference, a stretch of 1.5 corresponds to a Green-Lagrange strain of 0.625, where stretch, λ, is defined as

$$\lambda = l / l_0 \,. \tag{2.3}$$

2.2 Fluids

The fluid response was analyzed using an Arbitrary Lagrangian Eulerian (ALE) formulation. The governing field equations are,

Continuity:

$$v_{i,i} = 0 \qquad (2.4)$$

Momentum:

$$\rho \left[\delta v_i/\delta t + (v_j - \delta d_j/\delta t) \, v_{i,j} \right] = \tau_{ij,j} \qquad (2.5)$$

where

$\delta v_i/\delta t$ = the transient term of the particle velocities v_i at
  the position of the moving mesh point considered
ρ = constant mass density
d_j = the displacements of the moving mesh
$\delta d_j/\delta t$ = the velocities of the moving mesh
τ_{ij} = components of stress tensor:

$$\tau_{ij} = -p \, \delta_{ij} + 2\mu \, e_{ij} \qquad (2.6)$$

where

$e_{ij} = (v_{i,j} + v_{j,i})/2$
p = pressure
δ_{ij} = Kronecker delta
μ = fluid viscosity

and the gravitational term has been neglected. The boundary conditions used to solve these field equations are also discussed in *Section* 4.5.1.

3.0 Modeling Assumptions

The analysis was carried out in two phases, both of which were fully coupled fluid flow with structural interaction (FSI) analyses. In the first phase the fluid-structure model was brought to *in vivo* conditions, corresponding to a constant internal blood pressure and through-thickness arterial hoop stress, and a 1.5 axial arterial stretch ratio. The second phase was a restart analysis that used the results of the first phase's analysis as initial conditions. In the second phase a pulsatile physiological inlet blood pressure and flow rate were imposed on the model and its fully coupled transient response recorded. Three pulsatile cycles were computed to allow the model to attain a cyclic steady-state. The results from the third cycle are presented in the *Results* section of this paper.

The following modeling assumptions about the *in vivo* state of a carotid artery were incorporated into the finite element model, as mentioned in the *Introduction*:

1. *Constant through thickness arterial hoop stress at median blood pressure.*
2. *In vivo axial stretch of 1.5.*
3. *Non-linear material curve capable of large strains.*

In addition the stenosis was modeled as being stress-free when the artery was in its stretched and median blood pressure configuration. The remainder of this section will describe the motivation for these modeling assumptions and how they were incorporated into the analysis. The remaining modeling assumptions will also be given, as well as the parameter values that were used in the analysis.

3.1 Constant Through-thickness Arterial Hoop Stress

It is well established that the arterial wall undergoes active remodeling in such a way as to maintain an approximately constant through-thickness hoop stress at median blood pressure (Hayashi and Matsumoto (1996)). This physiological condition was modeled by applying a linear radial variation in initial hoop strain on the arterial wall. Green-Lagrange strain varied from negative 11.5 percent along the inner wall to 11.5 percent along the outer wall. This hoop strain variation in the artery's no-load state is verified experimentally and discussed at length by Fung (1993).

3.2 *In Vivo* Axial Stretch of 1.5

Arteries *in vivo* exhibit an axial stretch ratio of about 1.5 in the average healthy adult male, as referred to by Demiray (1988). The main purpose of the first phase of this analysis was to axially stretch the artery 40 percent so that once inflated at 100 mmHg the total axial stretch in the artery would equal 1.5. Ten time steps were used to stretch the artery by

applying an axial displacement at the downstream end of the artery while leaving both ends free to translate in the radial direction.

Two ALE mesh constraints were used to ensure that the fluid and solid meshes remained compatible during the analysis. In the first, the centerline of the fluid domain was defined to be a slip boundary, which eliminated the radial degree of freedom from the nodes on that boundary. In the second, six nodes along the centerline of the fluid mesh (five of which were in the stenosis region) were restricted to have the same displacements as six counterpart nodes on the solid model.

3.3 Stress-free Stenosis at Median Blood Pressure

The stenosis was modeled to be stress-free when the artery was in its stretched and distended median blood pressure configuration[i] depicted in Figure 1. This assumption was chosen in the absence of reliable experimental data on the longitudinal *in vivo* stress state of stenotic regions. The element birth and death options in *ADINA* were used to introduce a stress-free stenosis into the artery once the artery was in its *in vivo* median blood pressure configuration.

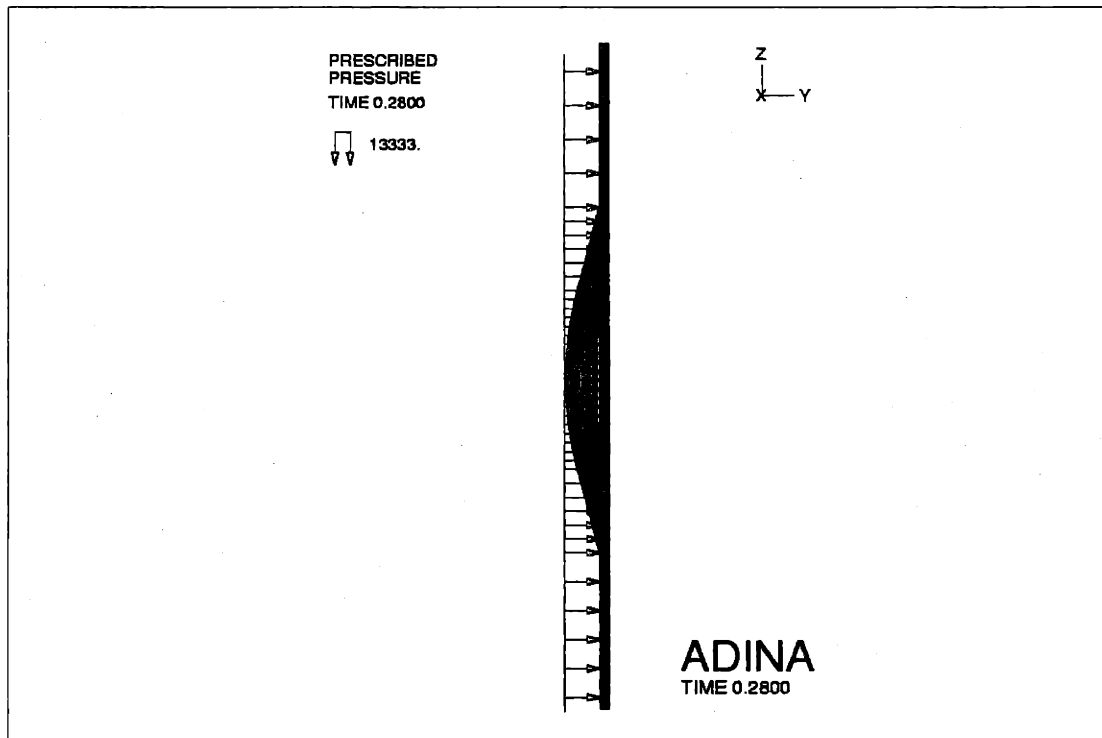PRESCRIBED PRESSURE
TIME 0.2800

13333.

ADINA
TIME 0.2800

Figure 1: Median blood pressure configuration, 30 percent constriction.

---

[i] The median blood pressure configuration implies that the artery is in the configuration that is reached by imposing a 100 mmHg pressure to the arterial wall, along the artery and *behind* the stenosis, as depicted in Figure 1 above.

To accomplish this two stenosis element groups were defined, each with its own material properties and life span[ii]. The first stenosis element group was a "dummy" element group with virtually zero stiffness. This element group was only active during the "prepping" stage of the analysis. It ensured that the stenosis nodes remained compatible with the artery during its deformations without affecting the artery's stress state. The second stenosis element group exhibited the actual physiological properties of the stenosis and was only brought to life once the artery was in its *in vivo* median blood pressure configuration. The physiological properties of the stenosis material were chosen to be five times stiffer than the arterial wall material (Born *et al.* (1989)), isotropic, incompressible, and homogeneous.

3.4 Non-Linear Large Strain Ogden Material Model

An experimental stress-stretch curve for the carotid artery of a dog, (Sato *et al.*, 1979) is shown in Figure 2 along with the fitted material curve used in this analysis. The highly non-linear nature of the material curve and the need for a material model that was capable of large strains of up to 60 percent were motivation for using an Ogden (1984) material model.
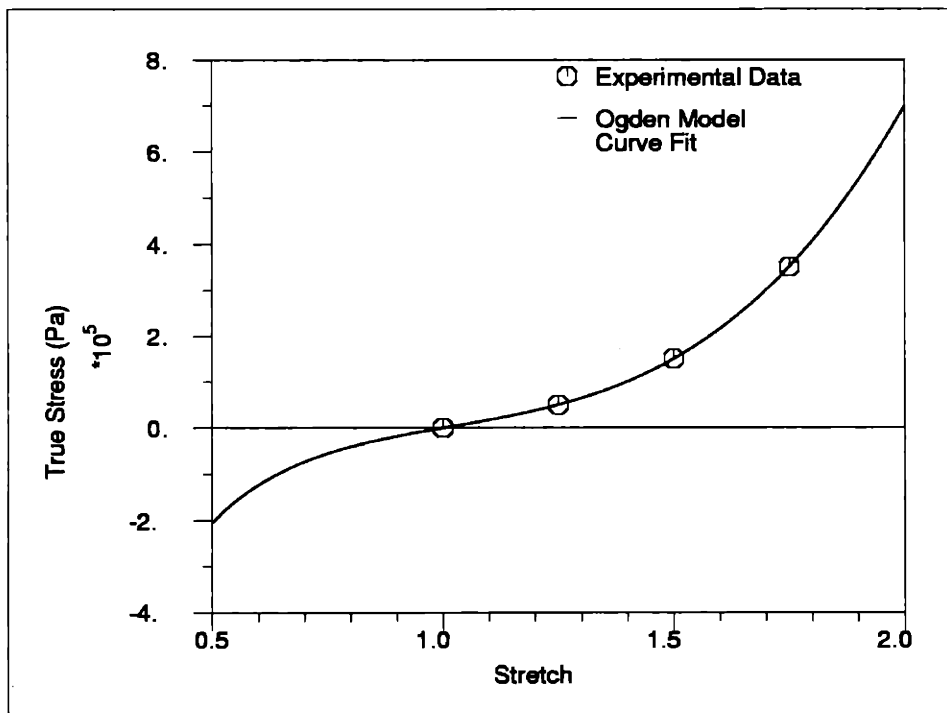

Figure 2: Experimental and fitted axial stretch-stress material curves.

[ii] The life span of an element group refers to the solution time span during which it is active.

The Ogden model is used to characterize a nonlinear hyperelastic material that is homogeneous, isotropic, and incompressible. The validity and limitations of treating the artery as homogeneous and isotropic are discussed elsewhere by Patel and Vaishnav (1972). The assumption of incompressibility is reasonable due to the high water content of arteries, as explained by Pedley *et al.* (1978). Incompressibility was incorporated into the model by setting the bulk modulus to be several thousand times larger than the shear modulus, Bathe (1996). The experimental stress-stretch curve was fit using a standard least squares approximation available in *ADINA*. Figure 2 shows that the fit is highly accurate to a stretch of 1.75, which is adequate for this analysis, in which the maximum stretches do not exceed 1.6. The artery was assumed to be 1.1 times as dense as water.

3.5 Remaining Modeling Assumptions

This simulation was intended to mimic conditions in the carotid artery, assumed to have an *in vivo* inner diameter of 4 mm and a 1:10 thickness to radius ratio. The computational domain included 7.25 diameters upstream of the stenosis and 17 downstream. The stenosis was assumed to be 2 inner diameters in length and to have an approximately sinusoidal geometry. The diameter at the narrowest point was assumed to be reduced by 30 and 80 percent (corresponding to area reductions of 51 and 96 percent, respectively) in the two models that were analyzed, representing a mild and severe stenosis.

The blood flow was assumed to be laminar in both the 30 percent and 80 percent constriction cases despite the relatively high peak stenosis Reynolds numbers of 940 in the 30 percent case and 580 in the 80. The limitations and implications of this assumption are discussed later in the *Discussion*. Blood was modeled as a homogeneous, incompressible, Newtonian fluid with constant properties, which is appropriate for larger arteries such as the carotid (Fung (1990)). Its density was assumed to be 1.1 E3 kg/m^3, and its laminar viscosity, 4E-3 kg/ms (Pedley (1980)).

3.5.1 Boundary Conditions

Solid

The kinematic assumption of axisymmetry used in this analysis eliminated all rigid body motions except translation in the axial direction. In both the initial and secondary phases of the analysis the artery ends were free to translate radially. Both ends were axially fixed during the secondary, pulsatile analysis, when the artery was in its stretched configuration. The assumption of free radial translation on the ends is valid because shear stresses in the *y-z* plane of the artery (ref. Fig. 1) are negligible in regions of ordinary stream-wise blood pressure gradients, present at both ends of the artery. The assumption of zero axial translation at the ends of the artery is appropriate due to the longitudinal tethering of fibers which restrict axial movements of the artery (Pedley (1980)).

Fluid

The assumption of axisymmetric flow eliminated the circumferential component of velocity throughout the fluid domain as well as the radial component at the centerline. A no-slip boundary condition was imposed at the fluid-structure interface, which is shown to be valid by Fung (1990) for viscous fluids such as blood. A physical traction formulation was used in *ADINA-F*, resulting in the following natural boundary conditions:

$$\tau_{ij} n_j = f_i^S \big|_S \tag{3.1}$$

where

$$\tau_{ij} = \text{fluid stress component } i,j$$
$$n_j = \text{components of the unit vector normal to the fluid boundary}$$
$$f_i^S = \text{components of the traction vector on the boundary}$$

3.5.2 Loading

The loading on the artery during the pulsatile analysis was entirely left to the fluid-structure coupling. The only user-defined structural loads that were imposed were those used to stretch and inflate the artery during the initial "prepping" stage of the analysis, discussed earlier.
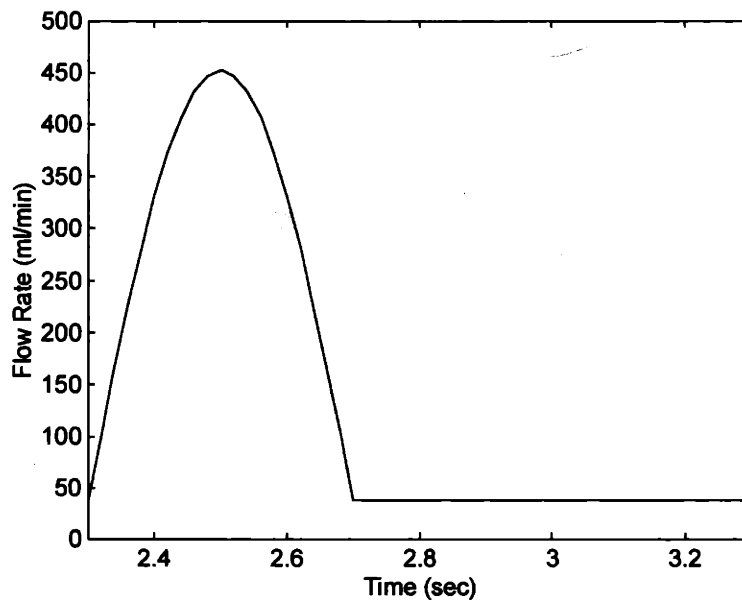
Panel A

Figure 3: 30 percent constriction prescribed inlet flow rate versus time for third pulsatile cycle (Panel A) and prescribed inlet pressure vs. time (Panel B).
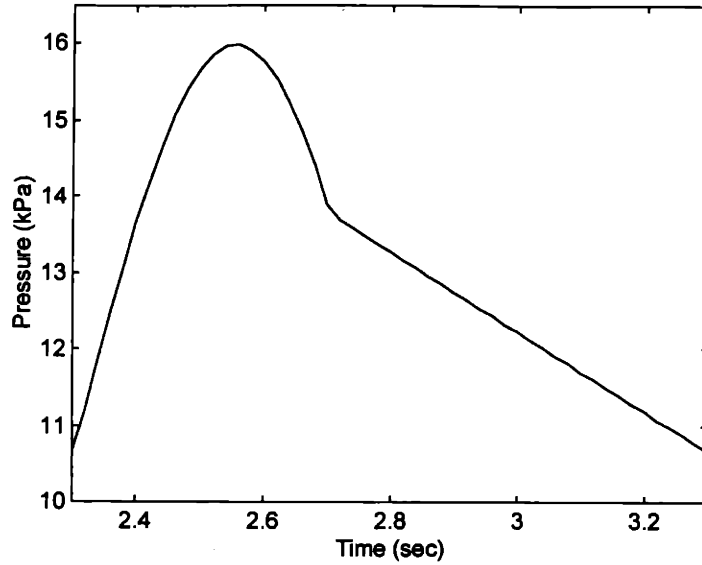
Panel B

During the three-cycle pulsatile analysis, only the inlet conditions were specified in the fluid. Both the inlet pressure and flow rate were specified as functions of time, each with a period of one second. The flow rate function depicted in Figure 3, Panel A, was imposed by prescribing a time varying centerline velocity and a parabolic inlet velocity profile. Note that the velocity profile entering a real stenosis would clearly be conditioned by arterial geometry at upstream locations. Seeing as this would be quite variable between subjects, a simple, straight, uniform inlet tube was chosen for this study. The pressure wave-form, which is approximated as initially sinusoidal followed by constant slope, is verified experimentally by Karamanoglu (1996) and depicted in Figure 3, Panel B. The prescribed inlet pressure and parabolic velocity functions were in phase with one another and are described mathematically by the following equations, where all units are in SI (*Pascals* and *meters*):

$$p(t) = 10.7\,E3 + 5.30\,E3 \cdot \sin(2\pi t) \quad (0 \le t \le 0.4) \quad\quad (3.2)$$
$$= 15.9\,E3 - 5.20\,E3 \cdot t \quad\quad (0.4 \le t \le 1)$$

$$w(r,t) = [0.55 \cdot \sin(2\pi t/0.8) + 50E\text{-}3] \cdot 8(a^2 - r^2)/D^2 \quad (0 \le t \le 0.4) \quad (3.3)$$
$$= 50E\text{-}3 \cdot 8(a^2 - r^2)/D^2 \quad\quad (0.4 \le t \le 1)$$

where

t = cycle time in seconds, based on a period of $T = 1$ sec
r = distance from centerline in coordinate radial direction (m)
$p(t)$ = fluid pressure (Pa)

14

$w(t)$ = axial velocity in the coordinate z-direction (m/s)

a = radius of artery at inlet at median blood pressure (m)

80 Percent Constriction Flow Reduction

The carotid artery is a cerebral artery that delivers blood to the brain. When it reaches the brain it narrows and branches off into many smaller vessels and eventually capillaries which allow it to deliver blood to different parts of the organ. It is known that the blood pressure in these capillaries and vessels never falls below about 15 to 30 mmHg. For this reason, it was assumed that the pressure at the exit of the artery, which was well after the pressure recovery downstream of the stenosis, could never fall below this physiological minimum. In the case of the 80 percent diameter reduction the flow through the stenosis was so highly constricted that it was necessary to reduce the normal flow rate function depicted in Panel A of Figure 3 by about a factor of five so that this minimum exit pressure, 30 mmHg, would not be breached. This assumption ensured that as long as the pressure recovery downstream of the stenosis was reasonable, the pressures in the stenosis region would also be accurate, leading to accurate stresses and strains in the plaque region.

3.5.3 Finite Element Model

Fluid

As mentioned briefly in *Section* 2.2 an Arbitrary Lagrangian Eulerian (ALE) formulation was used in this analysis (Bathe *et al.*, 1995). The ALE formulation is necessary when the fluid domain of a model changes, such as in the case of a free surface or FSI analysis such as this one. Figure 4 shows close-up fluid and solid mesh plots of the stenotic regions of the 30 and 80 percent constrictions. Axisymmetric, triangular three node fluid elements and a radially graduated fluid mesh were used with a higher element density near the arterial wall in order to capture the steep velocity gradient there, as seen in Figure 4.

Solid

A total Lagrangian formulation was used in this large strain, large displacement analysis to incorporate geometric and material nonlinearities into the model. A mixed displacement-pressure based finite element formulation was also used. This formulation is optimal for analyzing incompressible media, as described by Bathe (1996). Four node quadrilateral solid elements were used with a very high through-thickness density of 20 elements in the arterial domain in order to obtain an accurate solution (Fig. 4).
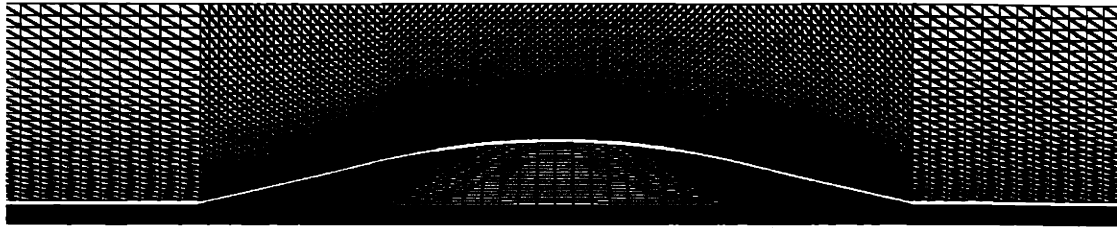
Panel A

Figure 4: Fluid and solid domain mesh plot close-ups of the stenosis region for the 30 percent (Panel A) and 80 percent (Panel B) constrictions.
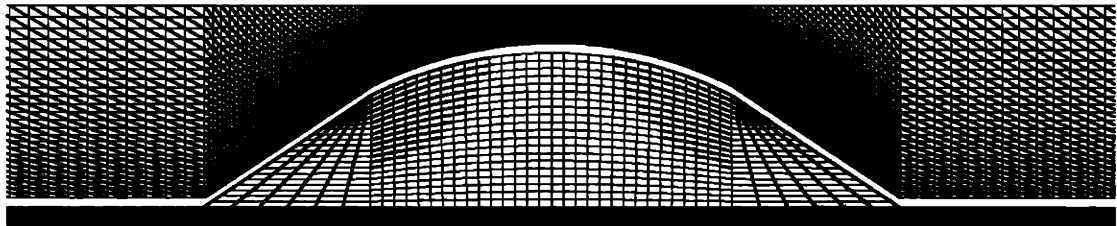
Panel B

4.0 Results

Only the results from the last pulsatile cycle, which ran from 2.3 sec to 3.3 sec, will be presented. Within this cycle three solution times were selected to illustrate different features associated with the stress and strain state in and around the stenosis. The first is 2.54 sec, when both the inlet pressure and flow rate are at a maximum, 16 kPa and 432 ml/min (91 ml/min in the 80 percent case). The second is 2.78 sec, the time of median blood pressure, 13.3 kPa, and minimum flow rate, 40 ml/min (8 ml/min). The third is 3.30 sec, when both the inlet pressure and flow rates are at their absolute minimums, 10.7 kPa and 40 ml/min (8 ml/min). In several of the following plots, axial position in the artery is plotted on the horizontal axis. In these plots the artery inlet corresponds to zero meters, the stenosis midpoint to 0.033 m, and the exit to 0.105 m.

4.1 Fluid

The transient blood pressure distribution in the immediate vicinity of the stenosis was the fluid result of primary interest in this study due to its dominating effect on the stress state of the stenosis region. For this reason, the 30 percent and 80 percent constriction axial pressure distributions will be presented for the three formerly mentioned time steps. The total pressure drop through the stenosis (including downstream recovery) will then be compared to existing experimental data in the *Discussion*, to gauge the validity of the model.
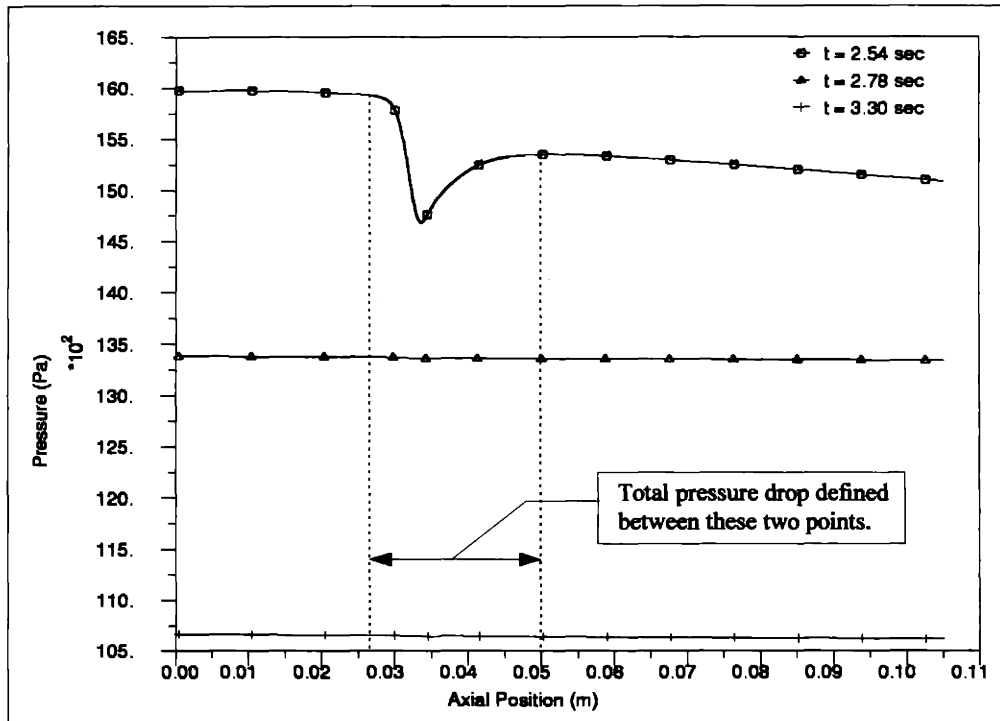
Panel A
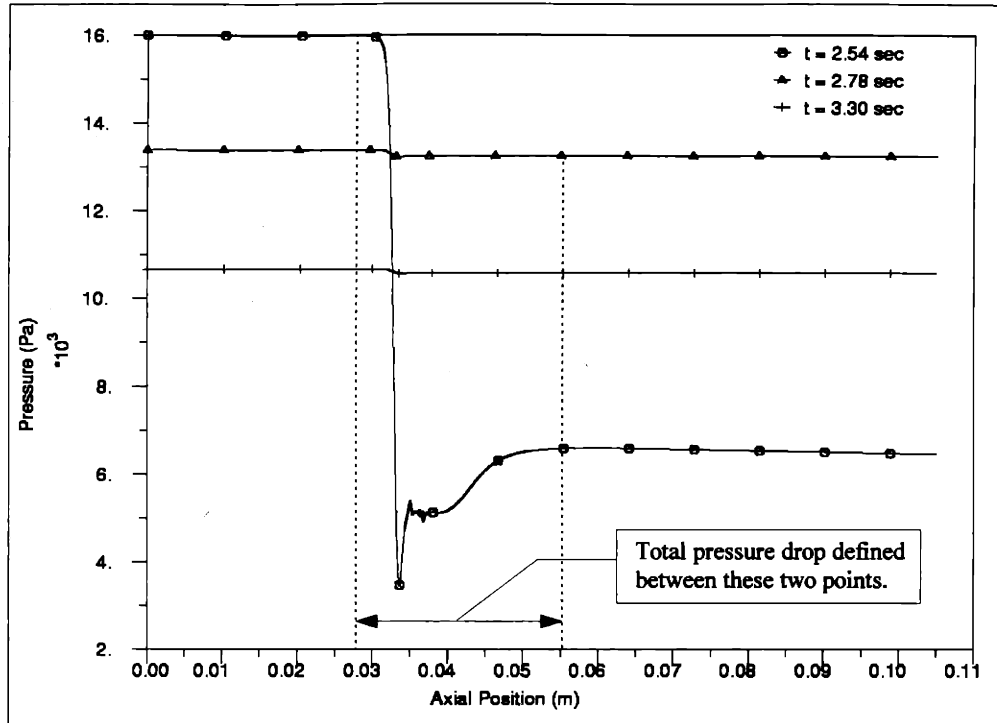
Panel B

Figure 5: Centerline blood pressure versus axial position for the 30 percent (Panel A) and 80 percent constrictions (Panel B). Artery inlet = 0 m, outlet = 0.105 m, stenosis midpoint = 0.033 m.

Axial Pressure Variation

Centerline blood pressure versus axial position is presented for both the 30 percent and 80 percent constriction cases in Figure 5, Panels A and B, respectively. In each case the total pressure drop, defined as the pressure just upstream of the stenosis minus the pressure downstream of the stenosis after pressure recovery, as depicted, is negligible for the low flow rate times (2.78 and 3.3 sec) when compared to that of the high flow rate time (2.54 sec). At the high flow rate time the pressure drop in the 30 percent case amounts to approximately 1.4 kPa, which is also small compared to the almost 13 kPa drop present in the 80 percent case. The total recoveries amount to 1 kPa and 3 kPa in the 30 and 80 percent cases, respectively. Total pressure recovery is seen to occur by an axial position of 0.050 m in the 30 percent case and 0.055 m in the 80 percent case. This corresponds to 3.25 and 4.50 diameters downstream from the end of the stenosis in the 30 and 80 percent cases, respectively. Seeing as 15 inner luminal diameters were modeled downstream of the stenosis, in both cases total pressure recovery occurred well before the artery exit.

4.2 Solid

4.2.1 Inner Wall Hoop Strain

Both spatial and temporal inner wall hoop strain results are presented in this section. Figure 6 shows the time variation of hoop strain at several points in the stenosis and artery and Figure 7 shows the axial variation of hoop strain at several discrete times within the cycle. As before, Panel A corresponds to the 30 percent constriction case and Panel B to the 80 percent one. Before reading these results recall that the Green-Lagrange strain representation used here is not equivalent to the commonly used stretch ratio, λ. As pointed out in *Section* 2.1, a stretch of 1.5 corresponds to a Green-Lagrange strain of 0.625.

Time Variation of Inner Wall Hoop Strain

In each Panel of Figure 6, the top graph shows the inner wall hoop strain history versus time for the far upstream and downstream end of the artery. The bottom graphs show the inner wall hoop strain histories for the stenoses. The plotted points include the endpoints of the stenoses, where the stenoses and arteries meet, as well as the midpoint of the stenoses, where the constrictions are at their maximums. Panels A and B show that in each constriction case the upstream end of the artery and stenosis have larger inner wall hoop strains than their downstream counterparts throughout the pulsatile cycle. This is simply a result of the stream-wise pressure drop in the flow, which is greatest across the stenosis. In both cases this difference is clearly largest during times of peak flow, which occurs at 2.54 sec (ref. Fig. 3, Panel A). In the 30 percent case the upstream hoop strain is seen to fall *below* the downstream strain for times between 2.65 and 2.73 sec. This is due to a negative trans-stenosal pressure drop that is induced by the deceleration of the flow during this time period, and will be further discussed in the *Discussion*.

The upstream arterial hoop strain histories seen in Panels A and B are the same in both constriction cases, each with an amplitude of 22 percent, due to their equivalent inlet pressure conditions. The downstream arterial amplitude is increased from 20 to 26 percent from the mild to severe constriction case and the downstream stenosal strain amplitude is increased from 4 to 4.5 percent, despite the larger, more rigid 80 percent stenosis.

In the 30 percent case in Panel A, the stenosis hoop strain is seen to oscillate around zero strain, as expected. Furthermore, as the flow rate is increased, the stenosis expands, as illustrated by the increasing hoop strain of the midpoint between times 2.3 and 2.6 sec. In the 80 percent case, however, the narrowest part of the stenosis is seen to get *narrower* as the flow rate is increased, as illustrated by the decreasing hoop strain of the stenosis midpoint between these same times. In fact, in the 80 percent case the midpoint and downstream end of the stenosis are in compression throughout the pulsatile cycle. The narrowing of the stenosis in the 80 percent case leads to a choking of the flow through the stenosis and will be discussed further in the *Discussion*.

19
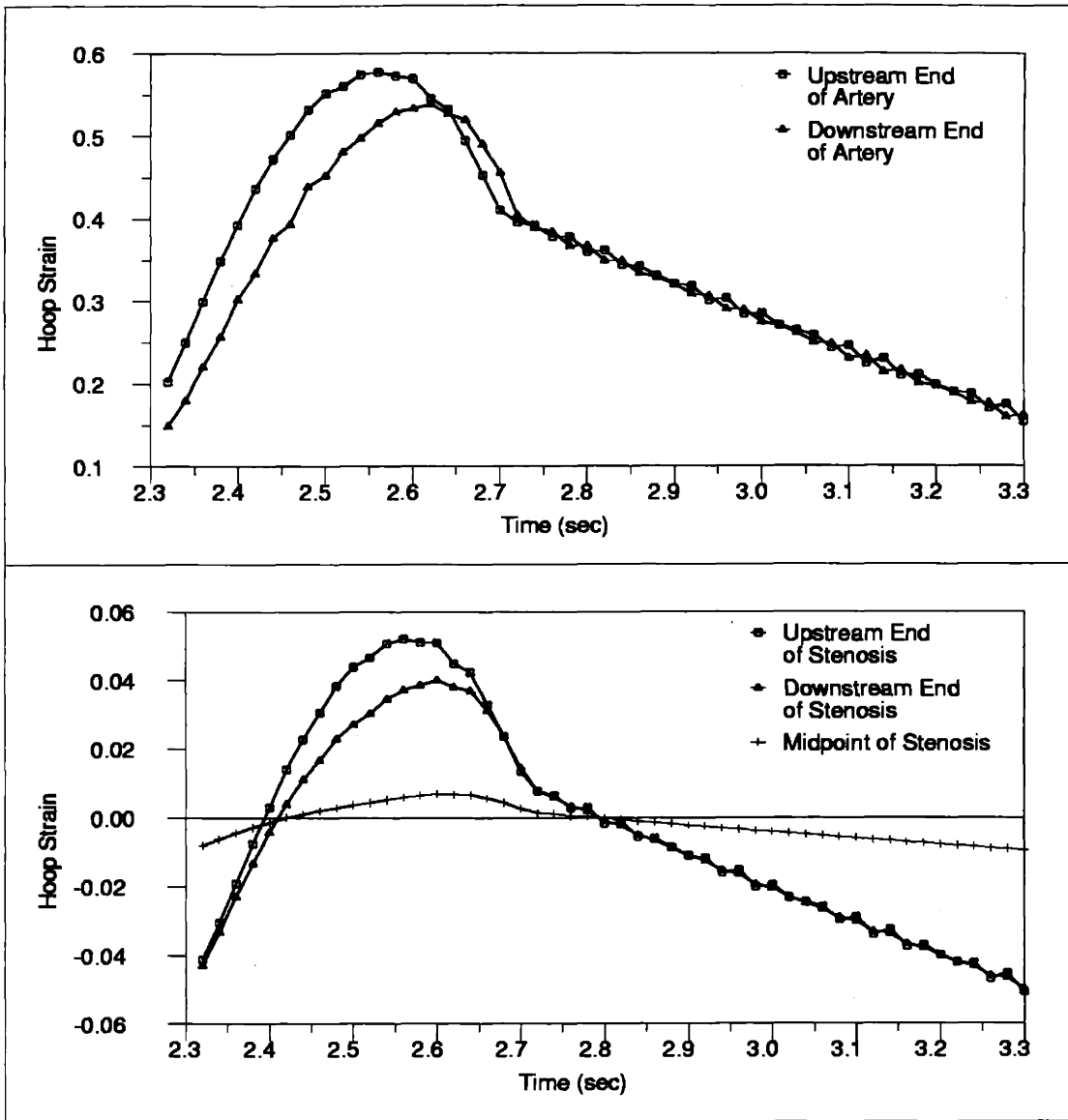
Panel A

Figure 6: Inner wall hoop strain versus time at the extreme artery ends (Top) and extreme stenosis ends and midpoint (Bottom) for the 30 percent (Panel A) and 80 percent (Panel B) constrictions.
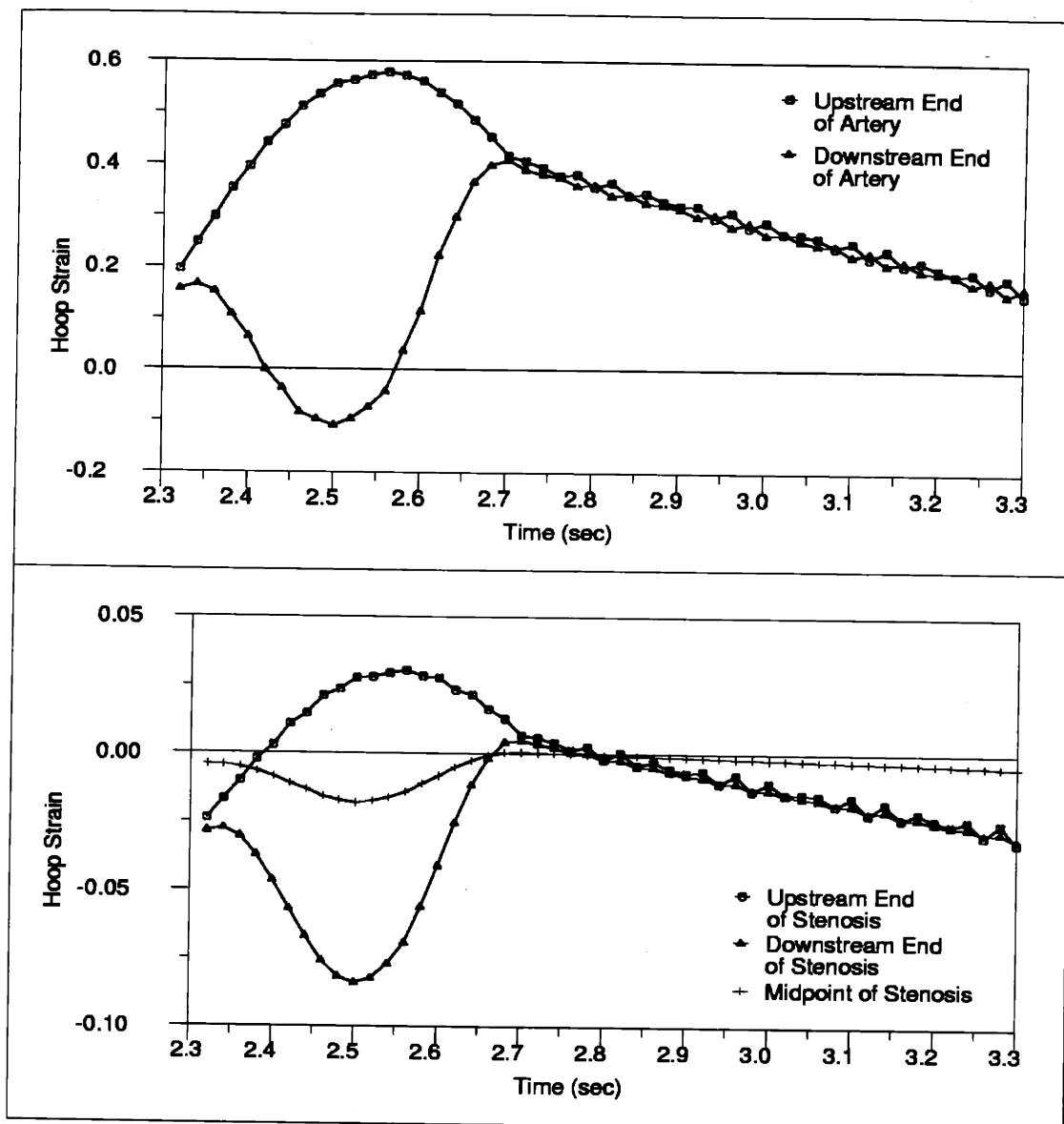
Panel B

Axial Variation of Inner Wall Hoop Strain

Panels A and B of Figure 7 show the axial distributions of inner wall arterial hoop strain for the 30 percent and 80 percent constrictions, respectively. In each case the distributions are plotted for the typical three solution times (2.54, 2.78, and 3.30 sec). The strain distributions are seen to closely resemble their counterpart blood pressure distributions shown in Figure 5, Panels A and B. In the 30 percent case the hoop strain is basically constant at 38 percent for the median blood pressure time step of 2.78 sec, when the trans-stenosal pressure drop is negligible due to the low flow-rate present at that time. At the peak flow-rate of 2.54 sec there is a more significant pressure drop through the stenosis (ref. Fig. 5, Panel A). This causes the 30 percent constriction arterial hoop strain

21

to fall from an upstream value of 57.5 percent to 53 percent downstream, with a noticeable axial gradient even in the unconstricted downstream region. At each time step the upstream hoop strain is again equivalent in both constriction cases, due to their equivalent pressure loading. At the high flow rate time step of 2.54 seconds the trans-stenosal pressure drop was seen to be very large in the 80 percent fluid results (ref. Fig. 5, Panel B). This result is evident in Figure 7 as well, where for the 2.54 time step the upstream to downstream hoop strain changes from 57.5 percent to a low of negative 10 percent, before recovering in conjunction with the blood pressure to about negative 7.5 percent.
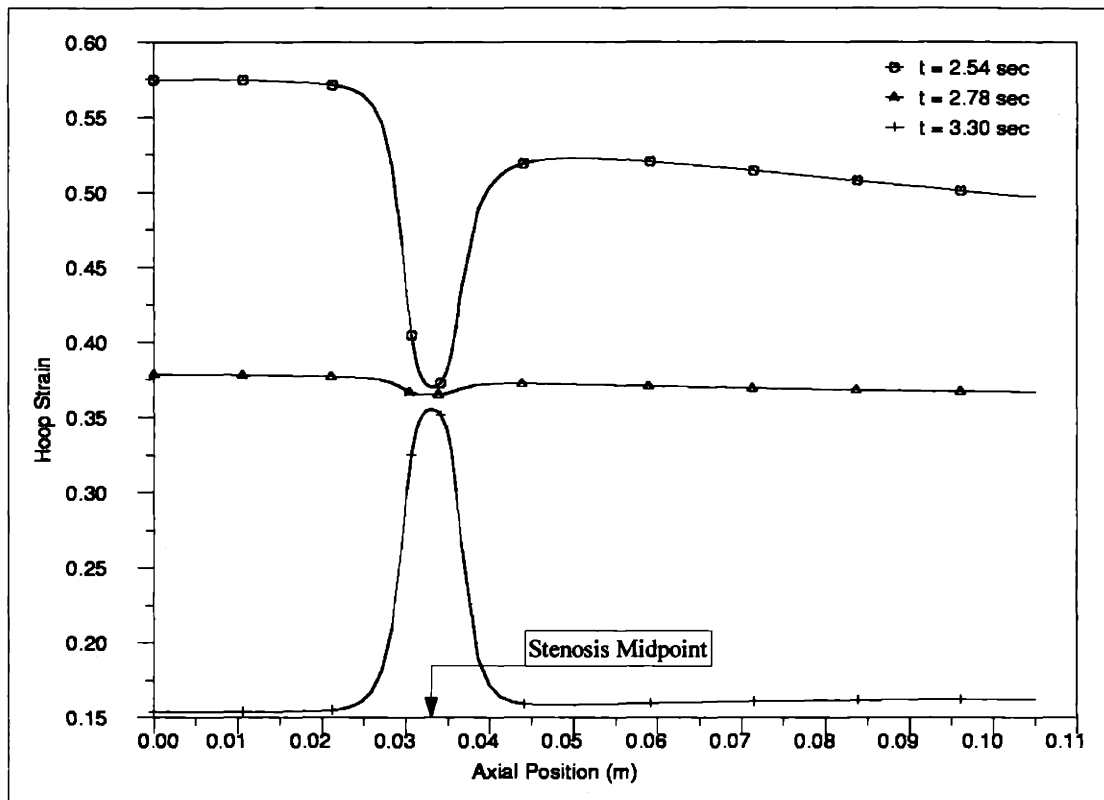
Panel A

Figure 7: Inner wall arterial hoop strain versus axial position at three time steps, 2.54, 2.78, and 3.30 sec for 30 percent (Panel A) and 80 percent (Panel B) percent constrictions. Artery inlet = 0 m, artery outlet = 0.105 m, stenosis midpoint = 0.033 m.
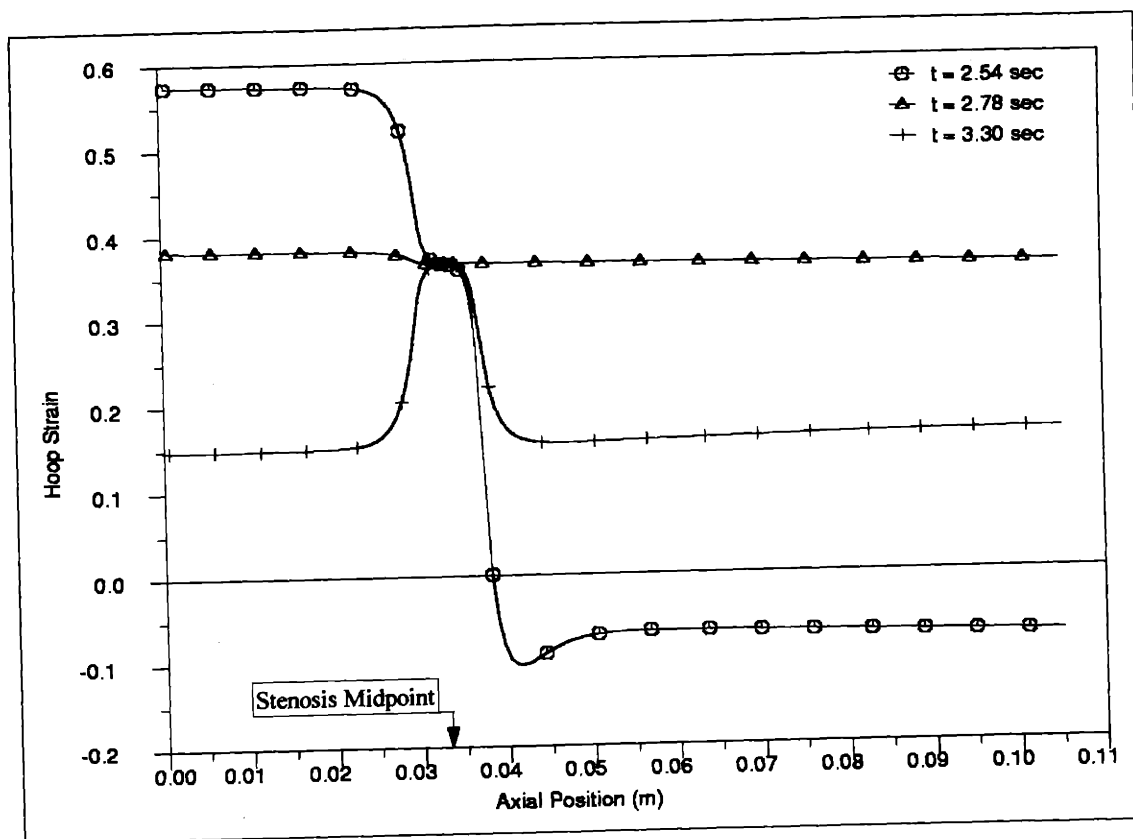
Panel B

In both the 30 percent and 80 percent constriction cases the arterial hoop strain in the stenosis region (0.033 m) remains relatively constant at its median blood pressure level of 37.5 percent due to the structural rigidity of the stenosis. The higher rigidity of the larger, 80 percent stenosis is evident in Panel B, however, where the inner wall hoop strain remains constant between times 2.54 and 3.30, compared to the 30 percent case in Panel A, where the strain is seen to vary by several percent between these times.

4.2.2 Stenosis Principal Stress and Hoop Strain

Panels A through D of Figure 8 show close-up color band plots of the hoop strain and maximum principal stress distributions in the stenotic regions during the time of peak flow and peak trans-stenosal pressure drop, 2.54 sec. Panel B shows that in the 30 percent case arterial principal stress remains constant at about 200 kPa from the upstream to downstream side of the stenosis, with a maximum of 226 kPa located further upstream of the region shown in the Figure. The arterial stress and outward radial deflection is reduced somewhat near the stenosis, where the stenosis bears the bulk of the internal pressure load. The principal stress in the 30 percent stenosis is seen to be at a maximum at the extreme upstream end where it reaches 36 kPa. The peak stress occurs at the upstream end of the 30 percent stenosis as opposed to the downstream end due to the

23

higher pressure there. The center of the stenosis is in compression, where the principal stress reaches a minimum of negative 10 kPa. The hoop strain distribution in the stenosis varies from a maximum of 5 percent at its upstream end to about zero at its center, where its rigidity does not allow any expansion, as expected.

80 Percent Stenosis Stress Concentration

Panel D of Figure 8 illustrates the large downstream arterial contraction present in the 80 percent case due to the large trans-stenosal pressure drop present at this time, as mentioned earlier. The contraction causes a compressive principal stress of 103 kPa in the downstream shoulder of the stenosis. This inward deflection is due to a combination of the artery's tendency to contract to its stress-free state, which occurs at a considerably smaller diameter than that which the stenosis forces it to maintain, and the large pressure drop present at this time of peak flow. Upon careful examination it can be seen that the artery expands back outward as the blood pressure recovers further downstream from the immediate vicinity of the stenosis, as was shown earlier in Panel B of Figure 7. The arterial hoop strain and principal stress fall considerably from the upstream to downstream side of the stenosis, where they have means of almost zero percent and 110 kPa, respectively, due to the low downstream pressure of approximately 4 kPa. The maximum principal stress and hoop strain in the artery are the same as they were in the 30 percent case, since these occur upstream of the stenosis where the pressure is equal in both cases.

STENOSAL
SMOOTHED
STRAIN-XX

RST CALC

TIME 2.540

0.04667
0.04000
0.03333
0.02667
0.02000
0.01333
0.00667

MAXIMUM
△ 0.05071

ARTERIAL
SMOOTHED
STRAIN-XX

RST CALC

TIME 2.540

0.5550
0.5250
0.4950
0.4650
0.4350
0.4050
0.3750

MAXIMUM
0.5748
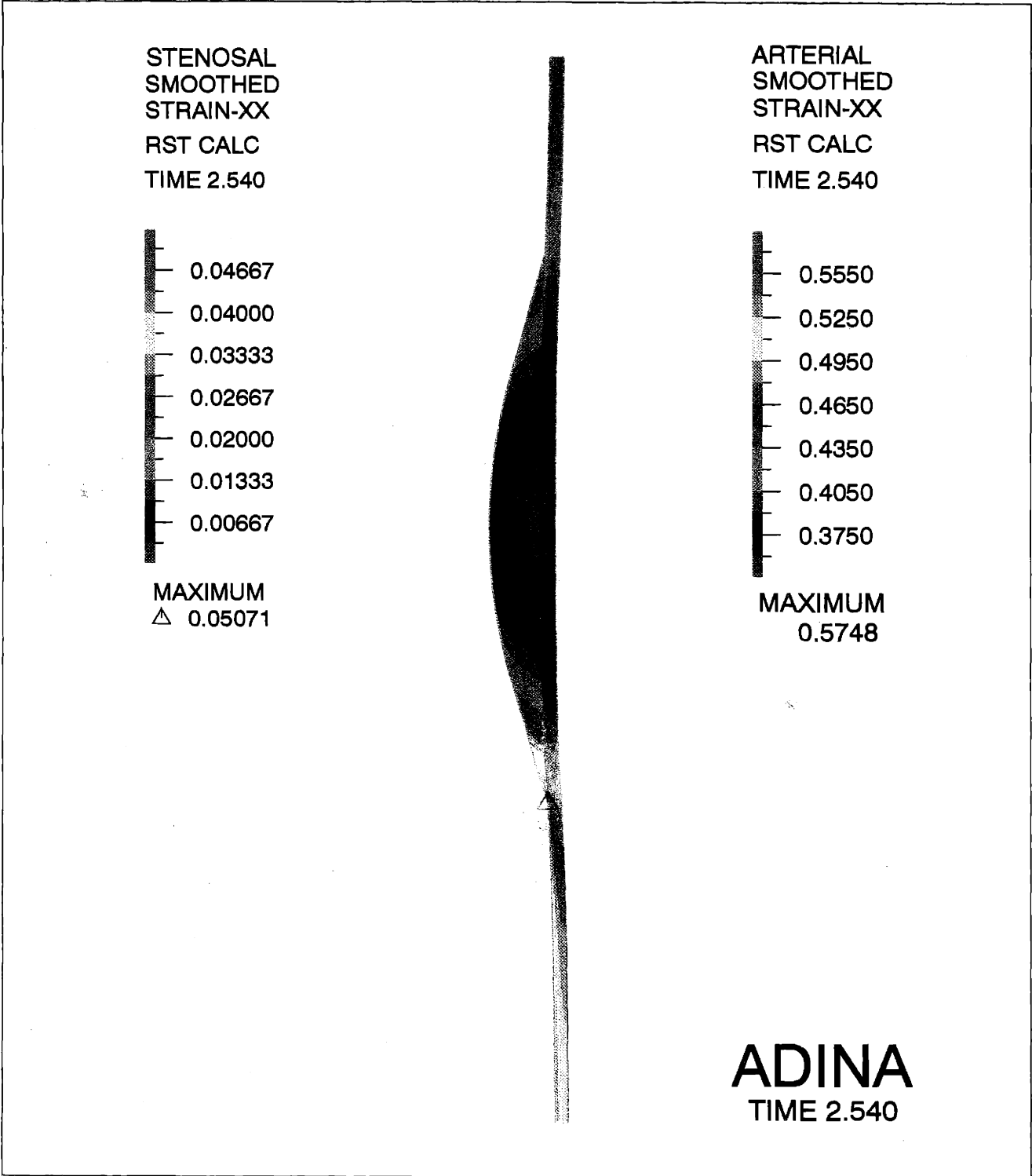
ADINA
TIME 2.540

Panel A: 30 percent constriction

Figure 8: Stenosis hoop strain and maximum principal stress (color).

STENOSAL
SMOOTHED
SIGMA-P1

RST CALC

TIME 2.540

33333.
26667.
20000.
13333.
6667.
0.
-6667.
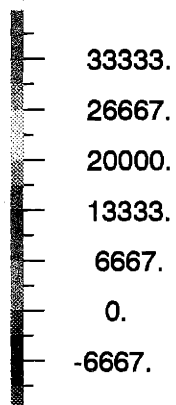
MAXIMUM
△ 35675.

ARTERIAL
SMOOTHED
SIGMA-P1

RST CALC

TIME 2.540

220000.
210000.
200000.
190000.
180000.
170000.
160000.
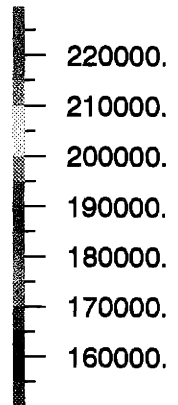
MAXIMUM
225692.

ADINA
TIME 2.540

Panel B: 30 percent constriction

26

STENOSAL
SMOOTHED
STRAIN-XX

RST CALC

TIME 2.540

0.02250
0.00750
-0.00750
-0.02250
-0.03750
-0.05250
-0.06750

MINIMUM
※ -0.07698

ARTERIAL
SMOOTHED
STRAIN-XX

RST CALC

TIME 2.540

0.5500
0.4500
0.3500
0.2500
0.1500
0.0500
-0.0500

MAXIMUM
0.5734
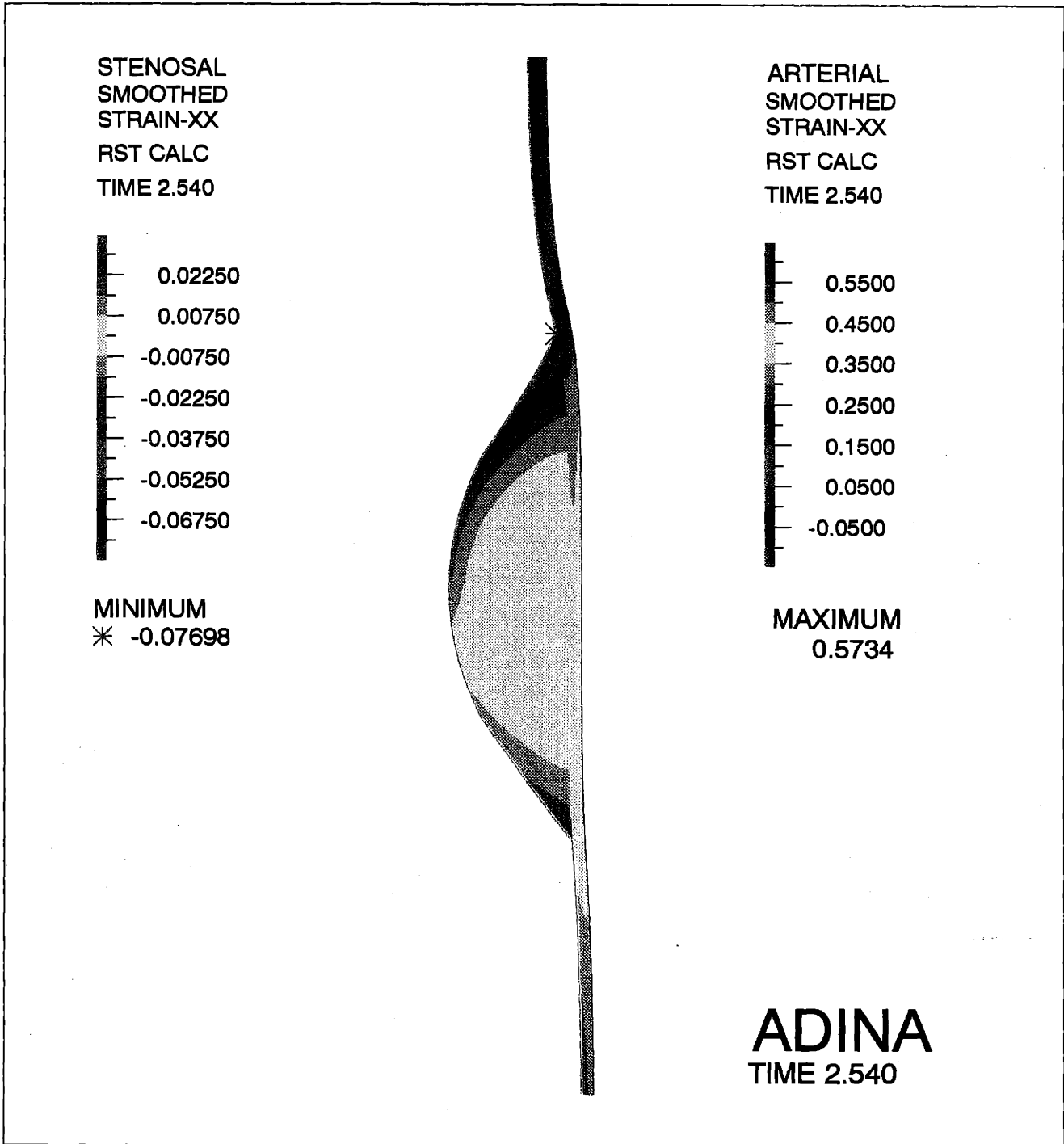
ADINA
TIME 2.540

Panel C: 80 percent constriction

STENOSAL
SMOOTHED
SIGMA-P3

RST CALC

TIME 2.540

-20000.
-33333.
-46667.
-60000.
-73333.
-86667.
-100000.
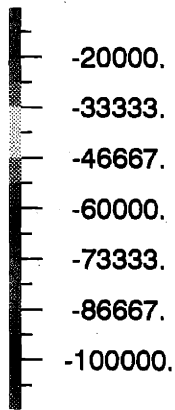
MINIMUM
✳ -102731.

ARTERIAL
SMOOTHED
SIGMA-P1

RST CALC
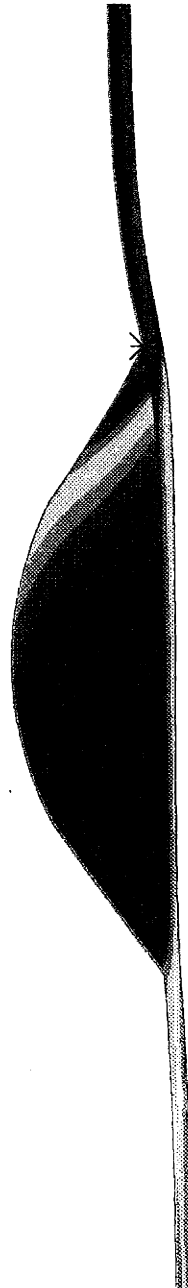
TIME 2.540

220000.
200000.
180000.
160000.
140000.
120000.
100000.
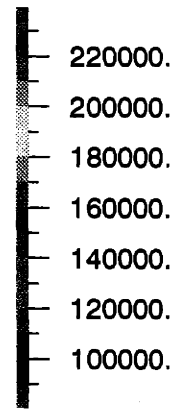
MAXIMUM
227485.

ADINA
TIME 2.540

Panel D: 80 percent constriction

5.0 Discussion

A new finite element model of a compliant stenotic artery has been developed. It is a fully coupled FSI model that incorporates a non-linear material curve, constant through-thickness hoop stress at median blood pressure, large strain analysis, a 1.5 axial arterial stretch ratio, and prescribed inlet blood flow and pressure conditions. The main limitations of the model are that it assumes axisymmetric geometry and loading, laminar flow, and a homogeneous, isotropic plaque and artery, leaving considerable room for future development of the model.

The main purpose of this study was to better understand the magnitude and nature of the transient stresses and strains present in and immediately around the plaque of a stenotic artery. It was also of interest to examine how these stresses and strains change with increasing severity of the stenosis. For this reason two models were analyzed, one with a relatively mild 30 percent diameter reduction and the other with a more severe 80 percent diameter reduction, corresponding to a 96 percent area reduction. Before the stress and strain results in and around each stenosis are to be trusted to be representative of *in vivo* conditions, it is critical to validate the transient pressure distributions computed in the regions. This will be done by comparing the total pressure drop across each stenosis to experimental data.

The peak upstream arterial Reynolds number in this analysis was 660 in the 30 percent case and 140 in the 80. While the assumption of laminar flow would clearly have been valid for a normal, unconstricted artery with these peak Reynolds numbers, the same is not true for a stenotic artery, where transition to turbulence can occur significantly earlier downstream of the stenosis due to the sudden area expansion there. In a steady-state experimental study of flow through a streamlined axisymmetric stenosis like the ones modeled here, Seeley and Young (1973) found that downstream transition to turbulence occurred at a Reynolds number of 800 in a 56 percent stenosis and 185 to 325 in an 89 percent one.

When turbulence is modeled in computational analysis, it is generally expected that a lower pressure recovery will occur downstream of a stenosis than in a laminar flow model and that therefore the total pressure drop across the stenosis will be greater. Since turbulence was not modeled in this analysis and the flow was close to the turbulent envelope found by Seeley and Young, albeit for steady flow, it is necessary to show that the pressure drop calculated in this study was accurate even though a laminar flow assumption was used. If the total pressure drop (defined in *Section* 4.1) computed in this analysis is shown to be comparable to experimental data, then the pressure distribution within the stenosis region can be trusted to be representative of *in vivo* conditions as well.

In order to validate the trans-stenosal pressure drop results computed in this analysis, they will be compared to an experimentally based steady-state formula derived by Seeley and Young (1976). First, however, the nature of pulsatile flow will be briefly discussed, and in

conjunction the use of a steady-state formula for verification of unsteady flow results will be validated.
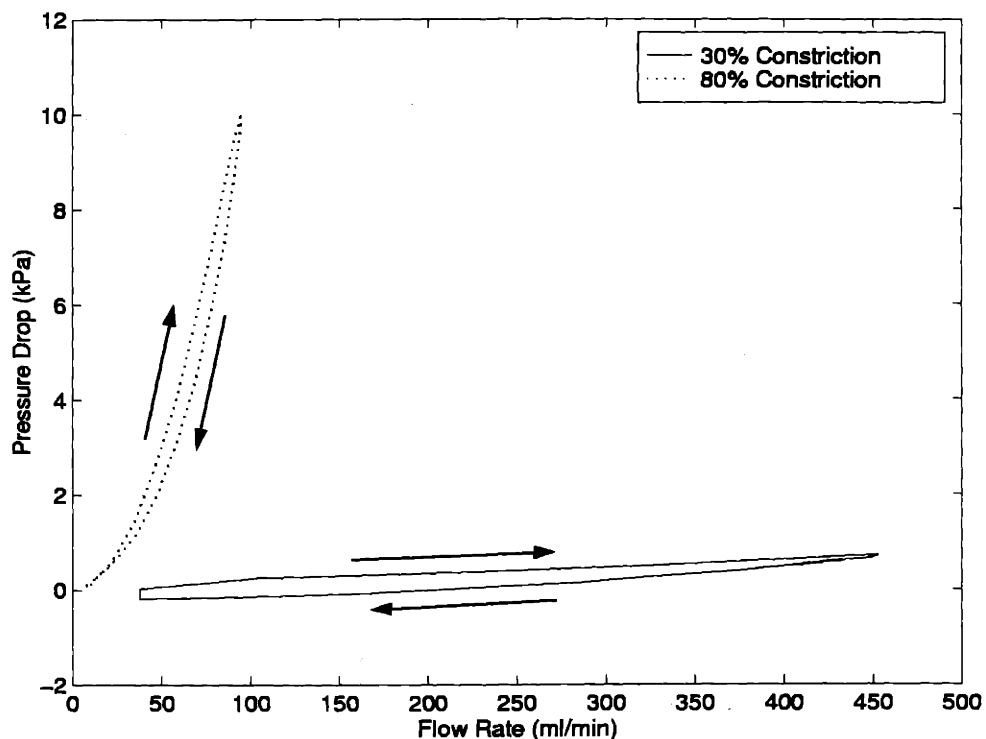
Figure 9: Upstream flow rate versus total trans-stenosal pressure drop (measured from upstream to after pressure recovery) for each constriction case.

Pulsatile Flow and Trans-Stenosal Pressure Drop

Upstream flow rate versus total trans-stenosal pressure drop is plotted for the two geometries in Figure 9. In each case, the pressure drop was calculated between upstream and downstream points where there was a constant axial pressure gradient. This is the same definition that was used in *Section* 4.1 of the *Results* section and corresponds to points 0.027 m and 0.050 m in the 30 percent constriction case (ref. Fig. 5, Panel A) and points 0.027 m and 0.055 m in the 80 percent case (ref. Fig. 5, Panel B), or ½ diameter upstream and 3.25 and 4.50 diameters downstream from the end of the plaque in each case. This definition of pressure drop includes the downstream pressure recovery.

The open loop pressure drop versus flow rate configuration observed in Figure 9, where two different pressure drops correspond to the same flow rate, was also observed in an experimental study performed by Campbell *et al.* (1996), and is primarily due to the acceleration and deceleration of the flow during the systolic and diastolic phases of the pulsatile cycle. In steady-state fluid flow a given pressure drop is needed to sustain a given flow rate. In unsteady flow a larger pressure drop is needed at a given flow rate to

accelerate a flow than is needed to decelerate it, as a consequence of Newton's First Law. The direction of increasing time is shown by the arrows in Figure 9. The other contributing factor to the open loop relationship seen in Figure 9 is the difference in velocity profile that exists during flow acceleration and deceleration. When a viscous fluid is accelerated the velocity gradient near the wall, $\partial V_z/\partial r \,|_{wall}$, tends to be greater than when it is decelerated. A higher velocity gradient means there must be a correspondingly higher wall shear stress resisting the flow, which means that a larger pressure drop is needed to drive the flow. As mentioned briefly in *Section* 4.2.1.1, in the 30 percent case these combined effects even cause the pressure drop across the stenosis to become negative at one point in the cycle, due to the relatively low flow rate (< 200 ml/min) and large deceleration present at that time.

The previous discussion leads us to believe that the steady-state pressure drop versus flow rate curve corresponding to the same geometry should lie in between the open loop pulsatile curves seen in Figure 9, since in steady-state the flow is neither accelerating nor decelerating. This result will be used next to compare the pulsatile flow results obtained in this study to the steady-state flow results obtained in two experimental studies performed by Seeley and Young (1976) and Tsai and Young (1973), thereby verifying to some degree this study's results.

The following equation was used by both Seeley and Young and Tsai and Young to correlate experimental data on the steady-state pressure drop through an axisymmetric stenosis:

$$\Delta p/\rho U_0^2 = (K_v/Re_0) + (K_t\,[(A_0/A_1) - 1]^2 / 2) \tag{5.1}$$

where U_0 is the average flow velocity in the unobstructed lumen, A_0 is the area of the unobstructed lumen, A_1 is the area of the narrowest part of the stenosis, Re_0 is the Reynolds number of the flow in the unobstructed lumen, and K_v and K_t are experimental constants which depend on the geometry of the stenosis, K_v depending much more heavily on geometry than K_t. The first term in Equation 5.1 accounts for viscous losses in the stenosis and the second term accounts for turbulent losses. For streamlined axisymmetric constrictions Seeley and Young found that the pressure drop is well predicted using

$$K_v = 32L(A_0/A_{1a})^2 / D_0 \tag{5.2}$$

and

$$K_t = 1.52 \tag{5.3}$$

where

$$A_0/A_{1a} = (0.75A_0/A_1) + 0.25 \tag{5.4}$$

For the geometry used in this finite element analysis, K_v was calculated to be 23,104 in the 80 percent constriction case and 203 in the 30 percent case. Seeley and Young recommend using 1.52 for the value of K_t, independent of geometry, whereas Tsai and

31

Young (1972) found that using a K_t of 0.9 predicted trans-stenosal pressure drop well for axisymmetric stenoses like the ones modeled here.

The experimentally determined dimensionless pressure drops, $\Delta p / \rho U_0^2$, versus upstream Reynolds number, $U_0 D_0 / \nu$, found by Tsai and Young (Theory A) and Seeley and Young (Theory B) are plotted in Panels A and B of Figure 10, along with the results from this study for the mild and severe stenosis.
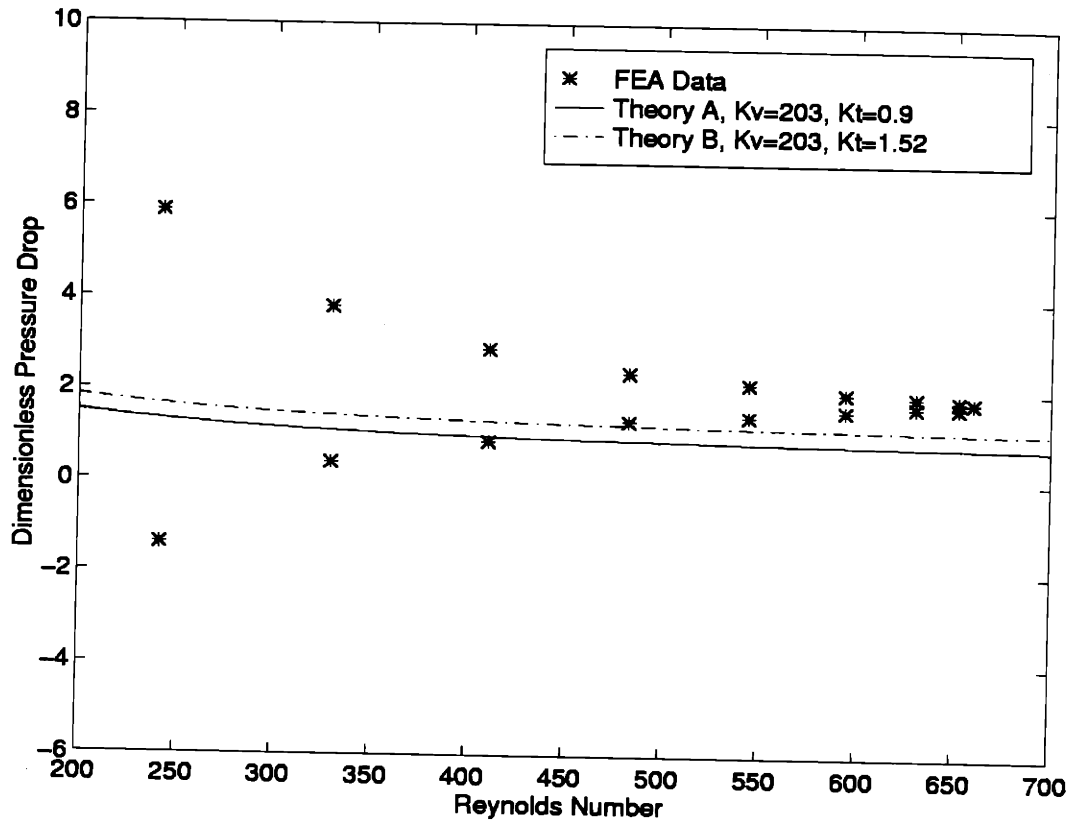
Panel A

Figure 10: Upstream Reynolds number ($U_0 D_0 / \nu$) versus dimensionless pressure drop ($\Delta p / \rho U_0^2$) comparison for 30 percent (Panel A) and 80 percent (Panel B) constrictions using two different experimental constants.

Panel A of Figure 10 shows that the FEA results for the 30 percent constriction agree well with the comparison experimental curves. The two experimental curves only differ by the difference in their constant turbulence terms, which is relatively small due to the mildness of the constriction. The decaying feature of the curves is due to the viscous term which approaches zero as the Reynolds number increases, leaving only the constant turbulent term. The fact that the FEA dimensionless pressure drop data lies above the experimental data implies that the computed pressure drop was larger than that found in the experiments, which means that the pressure recovery was smaller. In addition, the fact that for higher Reynolds numbers the FEA pressure drop results seem to become

independent of Reynolds number implies that the pressure drop is increasing with the square of velocity there, which is characteristic of turbulence. The fact that ADINA-F uses an upwinding scheme that effectively increases the fluid viscosity when the element Reynolds number is above two could account for this behavior.
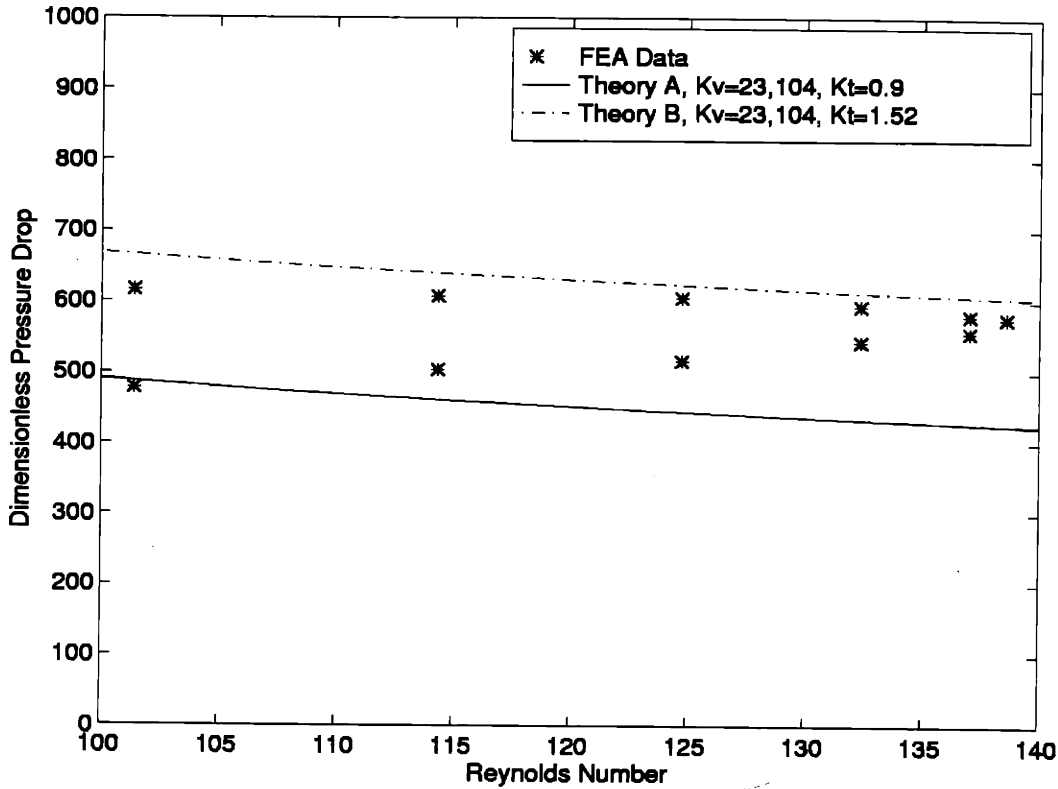
Panel B

The 80 percent constriction dimensionless pressure drop results are plotted in Panel B, where the pressure drop is seen to be much larger than in the 30 percent case, as expected, and the FEA data are seen to lie well within the bounds of error delineated by the two experimentally based curves. The slope of the experimental curves is significantly steeper than in the 30 percent case due to the fact that the viscous term has not decreased substantially by the Reynolds numbers shown. The relatively large constant difference between the two curves is again due to the constant turbulence term, although this time it is larger due to the higher percent stenosis and relatively larger importance of the turbulent pressure drop. As in the 30 percent case the FEA data behave as if turbulence is accounted for, probably due to the upwinding effect.

Due to the close agreement between the 30 percent constriction FEA data and the experimental curves in Panel A, it is concluded that despite the laminar flow assumption used in this study the pressure drop was computed accurately for that case. The

comparison of the 80 percent constriction results to experimental data does not lend as definitive a conclusion, however, due to the relatively large discrepancy between the experimental curves themselves and the fact that the FEA data lie in between the curves, it is also concluded that the pressure drop was computed sufficiently accurately in the 80 percent case.

Potential for Vessel Collapse and Accounting for Neglected Turbulent Effects

Vessels such as the carotid artery modeled in this study have been shown to be capable of post-stenotic collapse under *in vivo* conditions. Downing *et al.* (1997) demonstrated this phenomenon using a one-dimensional, unsteady flow model that accounted for frictional losses and Ku *et al.* (1993) demonstrated collapse of an axisymmetric compliant stenosis using a silicone rubber model.

In this study all post-stenotic pressures were found to be strictly positive throughout the pulsatile cycle. In fact, no negative pressures developed at any location in the fluid domain at any time during the cycle. The question then is was there any *potential* for negative post-stenotic pressures to develop at any time during the cycle? Succinctly, the answer is *no* in the 30 percent case and *yes* in the 80 percent one. In the 30 percent case the maximum trans-stenosal pressure drop was about 1.2 kPa. Given that this pressure drop was present when the upstream pressure was 16 kPa, and given the flat nature of the pressure drop versus flow rate curve in Figure 9, the possibility of negative post-stenotic pressures is clearly nonexistent, particularly since the comparative experimental study showed that the turbulent pressure loss neglected in this analysis was insignificant for this case. The same impossibility, however, is not present in the 80 percent case.

The highly resistive nature of the 80 percent diameter reduction stenosis is well-illustrated by Figure 9. The 30 percent curve lies flat, showing that the flow rate could be increased significantly without noticeably increasing the pressure drop through the stenosis. In the 80 percent case, however, the curve is much steeper and lies close to the pressure drop axis, highlighting the highly resistive nature of this constriction. A large increase in pressure drop is needed to achieve a small increase in flow rate. A significant contributing factor to this effect may be the actual narrowing of the stenosis that is caused by the downstream contraction of the artery, as mentioned in *Section* 4.2.1.1. There it was shown that the inner wall hoop strain at the midpoint of the 80 percent constriction stenosis was in constant compression throughout the pulsatile cycle (ref. Panel B, Figure 6). It should be noted here that whenever an axisymmetric solid model goes into compression, such as the 80 percent stenosis in this case, we must ask ourselves whether an axisymmetric model is still valid, since the model cannot account for non-axisymmetric buckling. Because the compressive hoop strains were relatively small and the stenosis relatively thick and hence rigid, it was probably accurate to assume an axisymmetric contraction in this case.

Returning to the resistive nature of the 80 percent stenosis. As mentioned in the *Modeling* section of this report the flow rate in the 80 percent case was reduced by a factor of 5 to

34

ensure that the arterial exit pressure would not drop below the physiological minimum of 30 mmHg imposed by downstream branching cerebral vessels and capillaries. A minimum of 30 mmHg was chosen as opposed to the more common minimum of 15 mmHg due to the possibility of neglected turbulence downstream of the stenosis, which would have resulted in a lower exit pressure than that which was computed in this study. Although the computed pressure drop was shown to compare well with existing experimental data, despite the laminar flow assumption that was used, the higher minimum exit pressure was retained to ensure that in the 80 percent case the physiological minimum exit pressure would not be breached. Therefore, this analysis represents a conservative scenario, where maximum turbulent dissipation is assumed to occur. In the extreme case of maximum dissipation, and hence zero pressure recovery, the minimum exit pressure in the 80 percent case would have been 3 kPa or 22.5 mmHg (ref. Fig. 5, Panel B), close to the more commonly accepted minimum of 15 mmHg, but still well above it.

The highly resistive nature of the 80 percent stenosis, along with the conservative estimate of minimum allowable exit pressure, combine to provide a high potential for negative post-stenotic pressures. Had the restriction on the minimum exit pressure been relaxed and the peak flow rate been increased by more than about 5 percent, it is very likely that negative post-stenotic pressures would have occurred, given the highly resistive nature of the 80 percent stenosis.

For this reason, in a future analysis using this model it should prove worthwhile to determine what the actual pressure recovery would be in the 80 percent case, so that under the laminar flow assumption a more appropriate minimum exit pressure could be used. That way a more accurate pressure distribution could be calculated, particularly in the region of the stenosis, where negative pressures are of interest. Even though turbulent models for low Reynolds number flows (such as this one) are presently unreliable, *ADINA-F* has several different options for modeling turbulent flow that could be used to calculate a more accurate downstream pressure distribution. The distribution could also clearly be determined using an especially designed experimental study. Another possibility would be to use a turbulent model for the entire pulsatile analysis, but given the increase in computation time needed to solve the additional two variables, and the unreliability of turbulent models, this option does not seem worthwhile.

Potential for Plaque Fracture or Fatigue

It is well established that lipid pools, particularly eccentric or non-axisymmetric ones, increase the tendency for atherosclerotic plaques to fissure, Born *et al.* (1989) and Cheng *et al.* (1993). Furthermore, the fissuring of a plaque containing a lipid pool is thought to be more dangerous than one without because lipid pools provide space for a large intraintimal thrombus to occur. A commonly accepted *minimum* stress required for fracture of atheromatous tissue is 300 kPa, as shown by Born *et al.* (1991).

In this study the plaque was modeled as homogeneous. Neither lipid pools nor calcification was accounted for within the axisymmetric plaque. This limitation in the

present model means that neither the large normal stress concentrations that have been found to occur adjacent to lipid pools, Cheng *et al.* (1993), nor the high shear stresses that have been found to occur adjacent to calcified plates could possibly occur in this model. This indeed was shown to be the case in the *Results* section where the peak principal stress was shown to be smooth throughout most of the plaque region in both constriction cases. The only significant stress concentration occurred in the 80 percent diameter reduction case, where there was a significant compressive stress of 103 kPa in the downstream shoulder of the plaque during times of peak flow. While this peak stress was well below the quoted plaque fracture stress of 300 kPa, it is clear that if lipid pools had been incorporated into the model, peak stresses in the plaque could very likely exceed 300 kPa due to the stress concentrating effects of the pool geometries. The location of this stress concentration on the downstream shoulder of the plaque, along with its cyclical nature, has been shown to set up a failure mode in plaques due to fatigue as well, (Ku *et al.* (1993)).

Stenosis Birth Assumption

The stenosis was assumed to be stress-free and strain-free when the artery was in its *in vivo* stretched and median blood pressure configuration. It is a subtle yet important point that the stenosis did bear the internal blood pressure load during the pulsatile analysis. That is, it was *not* stress-free when the internal blood pressure was 100 mmHg during the pulsatile analysis. The stress-free assumption was used due to the limited amount of experimental data available regarding the *in vivo* stress and strain distribution in and around a stenosis. The highest value in the stress-free assumption was that it provided a clear picture of what stresses were being caused by loading from the pulsatile blood flow.

The alternative to introducing the stenosis into the artery once it was in its *in vivo* state (ref. *Section* 3.3) was to include it in the model right from the beginning of the analysis. This alternative was investigated and proven to be inappropriate because of the plaque's high structural rigidity. The plaque caused large distortions in the surrounding artery after the stretching and inflating stage, so that once the artery reached its *in vivo* conditions, the plaque and surrounding artery region were already highly warped and stressed, thereby masking the transient stress distribution of interest, that which was caused by blood flowing through the artery.

Vessel Strain Amplitude

Arterial wall thickness varies widely across specimens. The range in canine carotid artery wall thickness to inner diameter ratio quoted by Pedley (1980) is 0.053 to 0.095, while the ratio used in this study was 0.050, which is just outside the range given by Pedley. The thin-walled artery assumption used in this analysis is the reason why the arterial hoop strain amplitudes are somewhat larger than those found in related studies.

The results of this study show that even a mild stenosis, such as the 30 percent diameter reduction analyzed here, has a significant impact on the hoop strains in a vessel. The 30

percent constriction almost fully restricted the normal vasodilation of the artery in the immediate region of the stenosis, and the 80 percent constriction not only fully restricted the local vasodilation of the artery but also increased the normal downstream inner wall hoop strain amplitude from 20 to 26 percent.

Sumpio has studied the effect of cyclic strain on endothelial cells, which line the inner wall of arteries, extensively. Amongst many other results, he has found that the production of endothelin, a vasoconstrictive molecule secreted by endothelial cells, increases five-fold over stationary conditions when the cells are subjected to 24 percent strain at 1 Hz (Sumpio and Widmann (1990)); that cyclic strain affects the overall gene expression and regulation of endothelial cell function (Sumpio *et al*. (1997)); and that cyclic strain causes a decrease in protein phosphatase 2A activity in the cytosol of endothelial cells (Sumpio *et al*. (1996)). The findings of Sumpio and other scientists establish the fact that endothelial cells are significantly affected by the presence, or absence, and magnitude, of cyclic strain. The findings of this study show that a mild stenosis of 30 percent diameter reduction can greatly influence the cyclic strain experienced by endothelial cells in the vicinity of the stenosis, and that a more severe stenosis of 80 percent can even have non-local effects on the cyclic strain experienced by endothelial cells well downstream of the stenosis. Therefore a stenosis can influence the normal biological function of endothelial cells by reducing, or in the case of a more severe stenosis increasing, the normal cyclic strain experienced by the endothelium.

Study Limitations

The limitations of this study include the assumptions of laminar flow, axisymmetry, and isotropy and homogeneity of the stenosis and artery. As previously mentioned, there is potential for the incorporation of a turbulent model such as the K-ε model into this finite element model. The reality, however, is that even with the *RNG* correction factor for low Reynolds number flows, which is available in *ADINA-F*, the K-ε model is unreliable, and therefore the benefits from abandoning the laminar flow assumption are not clear.

There are two main benefits that would come from abandoning the axisymmetric assumption used in this analysis and adopting a three dimensional model instead. The first is that non-axisymmetric stenosis geometries could be analyzed as well as non-axisymmetric lipid pools and regions of calcification included in the stenosis, which would provide a more realistic representation of the stress state in a stenosis. The second is that non-axisymmetric buckling of the artery and stenosis would be possible. This second benefit would clearly only be a benefit if the artery and/or stenosis had potential for non-axisymmetric buckling. Although the 80 percent stenosis was shown to be in compression throughout the pulsatile cycle, more definitive non-axisymmetric buckling tendencies would only arise if the minimum exit pressure used in this analysis was relaxed somewhat so that negative transmural pressures could possibly develop in the stenosis. The down side to a three dimensional model is that computation time could go up by a factor of 5 or more.

6.0 Conclusion

A new finite element model of pulsatile blood flow through a compliant stenotic artery has been developed and used to analyze a 30 percent and 80 percent diameter-reduced artery. Despite a laminar flow assumption, the computed trans-stenosal pressure drop is shown to be accurate through comparison to existing experimental data, affirming the accuracy of the computed stress and strain states in the regions of the stenoses. Results show that the inner wall of a healthy, unconstricted *in vivo* carotid artery undergoes large peak-to-peak hoop strain fluctuations on the order of 40 percent Green-Lagrange strain during the normal pulsatile cycle. The fluctuations are caused by the normal, uniform physiological pressure loading on the artery. It was also shown that even a 30 percent stenosis almost fully restricts the normal vasodilation of the artery, reducing inner wall hoop strain amplitude almost to zero in the immediate region of the stenosis.

No significant stresses developed in the stenosis in the 30 percent constriction case. In the more severe 80 percent constriction case, however, large downstream pressure reductions were induced in the artery during peak flow. The pressure reduction was large enough to cause a significant downstream arterial contraction, well beyond the normal physiological contraction of a healthy artery, resulting in an increase in inner wall hoop strain amplitude to 26 percent, from the normal 20 percent. This contraction also resulted in a cyclical compressive stress on the downstream end of the stenosis of 103 kPa. Finally, the 80 percent stenosis was found to be in compression throughout the pulsatile cycle, due to the abnormal downstream contraction of the artery, which increased the flow resistance of the stenosis by further reducing its minimum area.

7.0 Acknowledgments

8.0 Supplementary Material

A CD-ROM containing four *.htm* files and nine *.gif* files accompanies this thesis. The files are animated results from this finite element analysis. The fluid animations include axial fluid velocity, nodal pressure, and the stream function for both constriction cases. The solid animations consist of effective stress animations of the entire arterial model as well as close-ups of the upstream and downstream ends of the stenosis. Load the CD-ROM into a Windows 95 or NT based computer and open the *.htm* files in an Internet browser to view the animations.

9.0 References

Bathe, K.J., *Finite Element Procedures*, Prentice Hall Inc., New Jersey, 1996.

Bathe, K.J., Zhang, H., Wang, M. H., 1995, "Finite Element Analysis of Incompressible and Compressible Fluid Flows with Free Surfaces and Structural Interactions," *Computers and Structures*, **56**, No. 2/3: 193-213.

Bluestein, D., Niu, L., Schoephoerster, R. T., Dewanjee, M., K., 1997, "Fluid Mechanics of Arterial Stenosis: Relationship to the Development of Mural Thrombus," *Annals of Biomedical Engineering*, **25**: 344-356.

Born, G.V.R., Davies, M.J., Richardson, P.D., 1989, "Influence of Plaque Configuration and Stress Distribution on Fissuring of Coronary Atherosclerotic Plaques," *The Lancet*, October 21: 941-944.

Born, G.V.R., Davies, M.J., Lendon, C.L., Richardson, P.D., 1991, "Atherosclerotic Plaque Caps are Locally Weakened when Macrophage Density is Increased," Atherosclerosis, **87**: 87-90.

Campbell, C.S., D'Argenio, D.Z., Siebes, M., 1996, "Fluid Dynamics of a Partially Collapsible Stenosis in a Flow Model of the Coronary Circulation," *Journal of Biomechanical Engineering*, **118**: 489-497.

Caro, C.G., Pedley, R.J., Schroter, R.C., and Seed, N.A., *The Mechanics of the Circulation*, Oxford University Press, New York, 1978.

Cheng, G.C., Loree, H. M., Kamm, R. D., Fishbein, M. C., Lee, R. T., 1993, "Distribution of Circumferential Stress in Ruptured and Stable Atherosclerotic Lesions, A Structural Analysis with Histopathological Correlation," *Circulation Research*, **87**: 1179-1187.

Demiray, H., 1988, "Pulse Velocities in Initially Stressed Arteries," *Journal of Biomechanics*, **21**, No. 1: 55-58.

Downing, J. M., Ku D., N., 1997, "Effects of Frictional Losses and Pulsatile Flow on the Collapse of Stenotic Arteries," *J. of Biomechanics*, **119**: 317-324.

Du, W., Mills, I., Oluwole, B.O., Sumpio, B.E., 1997, "Gene Regulation by Mechanical Forces," *Endothelium*, **5 (2)**: 85-93.

Fung, Y.C., *Biomechanics: Mechanical Properties of Living Tissues*, Springer-Verlag, New York, 1993.

Fung, Y.C., *Biomechanics: Motion, Flow, Stress, and Growth*, Edwards Brothers, Inc., Ann Arbor, 1990.

Hayashi, K., Matsumoto, T., "Response of Arterial Wall Thickening to Hypertension and Residual Stress," *Biomechanics, Functional Adaptation and Remodeling*, Springer-Verlag, Tokyo, 1996.

Karamanoglu, M., 1997, "A System for Analysis of Arterial Blood Pressure Waveforms in Humans, *Computers and Biomedical Research*, **30**: 244-255.

Ku, D.N., McCord, B.N., (1993), "Mechanical Rupture of the Atherosclerotic Plaque Fibrous Cap," *ASME Bioengineering Conference*, ASME BED-Vol. **24**: 324-326.

Ku, D.N., Meister, J.J., Moore, J.E. Jr., Stergiopulos, N., Strassle, A., "Steady Flow Tests and Demonstration of Collapse on Models of Compliant Axisymmetric Stenoses," 1993, *Advances in Bioengineering*, ASME BED-Vol. **26**: 455-458.

Loree HM, Kamm RD, Stringfellow RG, Lee RT, 1992, "Effects of Fibrous Cap Thickness on Peak Circumferential Stress in Model Atherosclerotic Vessels," *Circulation Research*, **71**: 850-858.

Mills, I., Murata, K., Sumpio, B.E., 1996, "Protein Phosphatase 2A in Stretch-induced Endothelial Cell Proliferation," *Journal of Cell Biochemistry*, **63 (3)**: 311-319.

Ojha, M., Cobbold, R. S. C., Johnston, K. W., Hummel, R. L., 1990, "Detailed Visualization of Pulsatile Flow Fields Produced by Modeled Arterial Stenoses," *Journal of Biomedical Engineering*, **12**: 463-469.

Ogden, R.W., *Nonlinear Elastic Deformations*, Ellis Horwood, Chichester, U.K., 1984.

Patel, D.J., Vaishnav, R.N., 1972, "The Rheology of Large Blood Vessels," *Cardiovascular Fluid Dynamics*, **2**: 1-64.

Pedley, T.J., *The Fluid Mechanics of Large Blood Vessels*, Cambridge University Press, England, 1980.

Sato, M., Hayashi K., Niimi H., Moritake K., Okumura A., Handa H., 1979, "Axial Mechanical Properties of Arterial Walls and their Anisotropy," *Med. Biol. Eng. Comput.* **17**: 170-176.

Young, D.F., "Fluid Mechanics of Arterial Stenoses," 1979, *Journal of Biomechanical Engineering*, **101**: 157-175.

Seeley, B.D., Young, D.F., "Effect of Geometry on Pressure Losses across Models of Arterial Stenoses," 1976, *Joural of Biomechanics*, **9**: 439-448.

Sumpio, B.E., Widmann, M.D., 1990, "Enhanced Production of Endothelium Derived Contracting Factor by Endothelial Cells Subjected to Pulsatile Stretch," *Surgery*, **108 (2):** 277-281.